CONFIDENTIAL

Copy 233

RM A51H15

NACA

RESEARCH MEMORANDUM

LOAD DISTRIBUTION OVER A FUSELAGE IN COMBINATION WITH A SWEPT WING AT SMALL ANGLES OF ATTACK AND TRANSONIC SPEEDS

By Maurice D. White and Bonne C. Look

Ames Aeronautical Laboratory
Moffett Field, Calif.

NATIONAL ADVISORY COMMITTEE
FOR AERONAUTICS

WASHINGTON
November 27, 1951

CONFIDENTIAL

NATIONAL ADVISORY COMMITTEE FOR AERONAUTICS

RESEARCH MEMORANDUM

LOAD DISTRIBUTION OVER A FUSELAGE IN COMBINATION WITH A SWEPT WING AT SMALL ANGLES OF ATTACK AND TRANSONIC SPEEDS

By Maurice D. White and Bonne C. Look

SUMMARY

Free-fall tests were made of a wing-body configuration having a 45° swept-back cambered and twisted wing of aspect ratio 6 on a fuselage of fineness ratio 12.4. The test Mach numbers ranged from 0.85 to 1.06 and the Reynolds numbers from 2,750,000 to 5,600,000. The results of these tests indicated that over the entire test range of Mach numbers the fuselage in the vicinity of the wing (between stations 40 percent of the root chord forward of the wing leading edge and 80 percent of the root chord behind the wing trailing edge) carried a constant proportion of the total wing load amounting to 18 percent. Predicted values of the load carried over the fuselage in the vicinity of the wing based on subsonic and supersonic theories for a wing alone agreed with experimental values within 12 percent over the test range of Mach numbers. The change in distribution of load over the fuselage in the vicinity of the wing with increasing Mach numbers from 0.85 to 1.06 resulted in a rearward movement of the wing aerodynamic center of 5 percent of the mean aerodynamic chord. The distributions of load over the fuselage in the vicinity of the wing were similar to the distributions measured in wind-tunnel tests of other 45° swept-wing configurations despite differences in ratio of wing chord to fuselage diameter and in wing airfoil camber.

INTRODUCTION

The fuselages of supersonic aircraft are likely to be bigger in relation to the size of the lifting surfaces than those of subsonic aircraft. This fact makes it increasingly important to be able to assess accurately the distribution of load between the lifting surfaces and the fuselage.

Some experimental results that bear upon this problem are presented in references 1, 2, 3, and 4 for unswept wings and in references 3, 4, 5, and 6 for swept wings. References 1 and 2 present pressure distribution data only. References 3 and 4 demonstrate that the assumption commonly made for subsonic speeds, namely, that the fuselage contributes a lift approximately equal to that of the wing area projected through it, applies equally well at supersonic speeds for both unswept and swept wings. For swept-wing configurations, considerable data on the lift, drag, and pitching moments, supplemented by pressure distributions over the wing and fuselage are presented for Mach numbers up to about 0.96 in references 5 and 6 and for a Mach number of 1.2 in reference 6. The only published load results available for Mach numbers between 0.96 and 1.2 are in reference 4.

As part of an investigation being made at transonic speeds of a cambered and twisted wing swept back 45° some data were obtained on fuselage load distribution, the results of which are presented in this report. These results have been evaluated for an angle-of-attack range from -1° to +4° for Mach numbers from 0.85 to 1.06.

The data were obtained from free-fall tests of recoverable models conducted by the Ames Laboratory at Edwards Air Force Base, Muroc, California.

SYMBOLS

A	aspect ratio
b	wing span, inches
c	chord measured in streamwise direction, inches
$\bar{c}$	mean aerodynamic chord of total wing $\left(\dfrac{\int_0^{b/2} c^2 dy}{\int_0^{b/2} c\, dy} \right)$, inches
M	Mach number
$p_l - p_u$	difference in static pressure between lower and upper surface at a fuselage station, pounds per square foot
p_o	true ambient static pressure, pounds per square foot
p'	recorded ambient static pressure, pounds per square foot

Δp error in recorded ambient static pressure, pounds per square foot

q dynamic pressure, pounds per square foot

q_c recorded impact pressure, pounds per square foot

R Reynolds number of wing based on $\bar{c}$

r radius of the fuselage at station x, inches

S total wing area, square inches
(Total wing area is the sum of the exposed wing panel area and the fuselage plan area included by the projections of the wing leading and trailing edges to the fuselage center line.)

x longitudinal distance from station 0 of the fuselage, inches

y lateral distance from plane of symmetry, inches

α angle of attack, degrees

Λ sweepback angle, degrees

$\frac{\partial P}{\partial \alpha}$ load-coefficient slope $\left[\frac{(p_l - p_u)_{\alpha=4^\circ} - (p_l - p_u)_{\alpha=0^\circ}}{4q}\right]$

$\left(\frac{\partial C_N}{\partial \alpha}\right)_F$ normal-force-coefficient slope of fuselage in vicinity of wing

$$\left[\frac{1}{S\bar{c}} \int_{\text{station } 76.5}^{\text{station } 116} \int \left(\frac{\partial P}{\partial \alpha}\right) dx\, dy\right], \text{ per degree}$$

$\left(\frac{\partial C_N}{\partial \alpha}\right)_{FN}$ normal-force-coefficient slope of forward portion of fuselage

$$\left[\frac{1}{S\bar{c}} \int_{\text{station } 0}^{\text{station } 102} \int \left(\frac{\partial P}{\partial \alpha}\right) dx\, dy\right], \text{ per degree}$$

$\left(\frac{\partial C_L}{\partial \alpha}\right)_W$ lift-curve slope of exposed wing panels based on total wing area, S, per degree

$\left(\frac{\partial C_m}{\partial \alpha}\right)_F$ pitching-moment-coefficient slope of fuselage in vicinity of wing, based on total wing area and measured about quarter-chord point of wing mean aerodynamic chord, per degree

DESCRIPTION OF APPARATUS

Model

A three-view drawing of the free-fall model is shown in figure 1, and a photograph of the model is shown in figure 2. Pertinent physical dimensions are listed in table I. The model weighed 1316 pounds and was equipped with a dive brake and parachute to permit recovery of the entire model at the completion of the test period.

The fuselage was 210.5 inches in length and had a fineness ratio of 12.4. The fuselage was of semimonocoque construction except that between stations 121 and 146 a cylindrical tube served to carry the loads beneath the retracted dive brake. The fuselage ordinates from the 8-inch to the 139.4-inch station are given by the equation in table I. From station 139.4 the fuselage tapered conically to a radius of 5.2 inches at station 189.6. From stations 189.6 to 210.5 a tail shape approximating that given by the equation was used. The recovery parachute was carried in the section behind the tail surfaces.

The wing was swept back 45° at the quarter-chord line and had an aspect ratio of 6.0, a taper ratio of 0.49, and the airfoil section perpendicular to the quarter-chord line was the NACA 64A810 with a modified $a = 0.8$ mean line. A washout of 10° at the tip (measured streamwise) was obtained by twisting the wing so that the constant-percent-chord lines remained straight. The wing was machined from solid aluminum alloy. A rubber seal of approximately tubular cross section was cemented to the wing surface and to the internal side of the fuselage skin to prevent air flow through the gap between the wing and the fuselage.

Both horizontal and vertical surfaces were all-movable, pivoting on axes perpendicular to the fuselage axis. The horizontal-tail movement was programmed to deflect and return the tail to trim position impulsively at regular time intervals. The vertical tail surfaces were actuated differentially by the roll-stabilization system to provide roll control.

Instrumentation

Pressure orifices flush with the skin were located at the fuselage stations denoted in figure 3. Corresponding orifices on the upper and lower surfaces of the fuselage were connected to opposite sides of the pressure cells to record the difference in pressure between the two orifices for the wing-on tests. Individual pressures on the upper and lower surfaces were measured in the wing-off tests.

A wing balance using strain gage elements was installed in the fuselage to measure the lift and drag forces and pitching moments on the exposed wing panels.

The SCR 584 radar installation of the NACA High-Speed Research Station at Edwards Air Force Base was used for the airspeed calibration.

NACA recording instruments were used to measure airspeed, altitude, pressure differences between orifices, rates of pitch and roll, and angles of attack and sideslip. The records were synchronized by means of a chronometric timer. Other instruments were mounted in the body for other phases of the tests; only those pertinent to the results in this report are mentioned here. The sensing vanes for the angle-of-attack and sideslip-angle determination are shown in figures 1, 2, and 4.

The carrier airplane was an Air Force photo reconnaissance airplane that was specially adapted for the drop model program. The airplane was equipped with NACA recording instruments in order to measure airspeed, altitude, and free-air temperature during the climb prior to release of the model. These measurements, in conjunction with radar records, comprised the survey which was a necessary part of the airspeed calibration as mentioned in a later section of this report. Additional instrumentation to perform predrop checks of the model was also included in the airplane.

TESTS

The drop model was released from the carrier airplane at an altitude of 40,000 feet and allowed to free-fall to an altitude of about 18,000 feet where recovery was initiated. Recovery was effected by opening the dive brake to decelerate the model to a speed at which the recovery parachute could be released. During the entire drop up to the initiation of recovery, continuous records were obtained on all the recording instruments.

In the tests reported herein, the horizontal stabilizer was preset at release to maintain a model angle of attack corresponding to approximately zero lift for the wing. After a Mach number of about 0.85 was reached, the horizontal tail was moved in accordance with a preset program; at 2.4-second intervals the tail was deflected briefly and returned to its original trim setting. The resulting oscillations of the model covered an angle-of-attack range from -1° to $+4^{\circ}$, and occurred over a Mach number range from 0.85 to 1.06 and a Reynolds number range from 2,750,000 to 5,600,000. A typical time history showing the variation of recorded Mach number, altitude, and model Reynolds number during the free-fall is shown in figure 5.

The airspeed calibration was made by the method described in reference 7. This method consists of comparing, at a common geometric altitude, the static pressure recorded by the airspeed system of the falling model and the correct static pressure as recorded in the carrier airplane during the climb. The geometric altitude is determined by radar measurements. The results of the airspeed calibration are presented and discussed in appendix A.

ACCURACY OF RESULTS

Based on the sensitivity of the recording instruments and the repeatability of results from different drops, the following estimated errors may be assigned to the results:

	M = 0.85	M = 1.05
Mach number, M	± 0.01	± 0.01
Load-coefficient slope at a point, $\partial P/\partial \alpha$	$\pm .006$	$\pm .002$
Normal-force-coefficient slope, $(dC_N/\partial \alpha)_F$	$\pm .0018$	$\pm .0006$
Pitching-moment-coefficient slope, $(\partial C_m/\partial \alpha)_F$	$\pm .0014$	$\pm .0005$

RESULTS AND DISCUSSION

Loads and Pitching Moments

The results presented in this report are based on the load-coefficient slope, $\partial P/\partial \alpha$, which was evaluated using the relationship

$$\frac{\partial P}{\partial \alpha} = \frac{(p_l - p_u)_{\alpha=4^\circ} - (p_l - p_u)_{\alpha=0^\circ}}{4q}$$

The pressure data were reasonably linear with angle of attack over this range of angles of attack, which permitted interpretation of the results as slopes rather than as finite increments over a particular angle-of-attack interval. Values of the parameter $\partial P/\partial \alpha$ for the various fuselage stations were integrated over the area between stations 76.5 and 116 in order to obtain values of the normal-force-coefficient slope $(\partial C_N/\partial \alpha)_F$ and values of the pitching-moment-coefficient slope $(\partial C_m/\partial \alpha)_F$.

In figure 6, the curve labeled "fuselage in vicinity of wing" shows the variation with Mach number of $(\partial C_N/\partial \alpha)_F$ as determined by this integration. In assessing these results, it may be considered that the values shown represent the increment in load due to the wing because the load over this region was very small with the wing off. This is shown by the data of figure 7 where for several Mach numbers the longitudinal distribution of load over the fuselage center line for the present tests is compared with similar data obtained in preliminary tests with the wing off. It is also indicated by the data of figure 7 that the fuselage area covered by the orifices used in the wing-on tests comprises nearly all the area influenced by the wing, the values of $\partial P/\partial \alpha$ for the wing-on tests approaching measured or extrapolated values from the wing-off tests at the extremities of the area covered by the orifices.

Figure 6 also shows the variation with Mach number of the lift-coefficient slope of the exposed wing panels as measured by a balance within the model, and the load-coefficient slope for the forward part of the fuselage as determined from wing-off pressure measurements at an angle of attack of about 5°. In the wing-off tests an elliptical transverse distribution of loading was assumed in conjunction with the pressures measured along the center line of the body to establish the loading over the forward part of the fuselage.

The wing area within the fuselage comprises 24 percent of the total wing area. The load carried by the fuselage in the vicinity of the wing

represents about 18 percent of the total wing load[1] throughout the test Mach number range, including transonic Mach numbers. The ratio 18/24 = 0.75 may be considered as equivalent to the ratio of the average local additional lift coefficient to the total additional lift coefficient, which may be denoted as c_l/C_L. The theoretical values of c_l/C_L for this region of a plain wing would be calculated from reference 8 as 0.85 for all subsonic Mach numbers up to about 0.975, and from reference 9 as 0.79 for a Mach number of 1.05. The agreement of the theoretical results from references 8 and 9 with the flight value of c_l/C_L of 0.75 is remarkably good considering that the theories are for a plain wing without a fuselage, and considering that the comparisons are being made for Mach numbers very close to 1.0 where such theories are not expected to be applicable. Since the agreement may be only fortuitous the formulation of conclusions regarding the general applicability of the theories at Mach numbers close to 1.0 or at higher angles of attack should await further comparisons with experimental results.

The loading over the forward part of the fuselage contributes an additional load of about 12 percent of the total wing load.

The variation of $(\partial C_m/\partial\alpha)_F$ with Mach number is shown in figure 8. The curve shows a rather smooth variation in $(\partial C_m/\partial\alpha)_F$ with Mach number, the value decreasing by about 0.004 as the Mach number increases from 0.85 to 1.05. This change in value of $(\partial C_m/\partial\alpha)_F$ is equivalent to a rearward movement of the aerodynamic center of the total wing of 5-percent mean aerodynamic chord. The change in aerodynamic-center location with Mach number is due primarily to progressive rather than abrupt changes in pressure at the individual orifice stations. This is demonstrated by the data shown in figure 9 where the values of $\partial P/\partial\alpha$ for the individual orifice stations are plotted as a function of Mach number. The forward stations show a generally progressive decrease in value of $\partial P/\partial\alpha$ and the rearward stations show a generally progressive increase in value of $\partial P/\partial\alpha$ with increasing Mach number. These progressive trends account for about three-quarters of the aerodynamic-center shift noted. The remainder of the shift is probably attributable to the abrupt changes in loading at stations near the leading edge and trailing edge of the wing root.

The abrupt increases in value of $\partial P/\partial\alpha$ at the stations in the vicinity of the wing trailing edge at the root are similar to abrupt increases in this region that were reported in reference 6. In reference 6, it was shown that the pressures over the fuselage in this region corresponded closely to the pressures over the wing adjacent to these stations. Reference 6 showed that at the forward stations the wing and

[1]"Total wing load" is defined as the load over the exposed wing panels plus that over the fuselage plan area between stations 76.5 and 116.

fuselage pressures were quite dissimilar. The abrupt decreases in the value of $\partial P/\partial \alpha$ at the leading-edge stations in figure 9 are believed to be associated with the passage of shock waves emanating from the juncture of the wing leading edge and the fuselage.

Load-Coefficient Distribution

The distribution of loading along the fuselage in the vicinity of the wing is shown in figure 10 for several Mach numbers from 0.90 to 1.05. Over this range of Mach numbers the distributions show little change with Mach number except near the wing leading edge.

Comparisons are made in figure 10 with wind-tunnel data for wings having 45° of sweepback as obtained from references 5 and 6. Subsonic data from both references are compared with flight data for $M = 0.90$. Data from reference 6 for Mach numbers of 0.96 and 1.20 are shown with flight data for Mach numbers of 0.975 and 1.05, respectively.

The data of figure 10 show reasonably good agreement between the flight results and the wind-tunnel results at the Mach numbers considered. This is particularly significant in view of the fact that there were large differences in ratio of wing chord to fuselage diameter and in airfoil section between the configurations used in the flight and in the wind-tunnel investigation. The relative insensitivity of the results to changes in airfoil section and in wing-fuselage size suggests that the data presented in this report and in references 5 and 6 may be used to predict the transonic loading distributions for a wide class of configurations.

Comparisons are also included in figure 10 of the theoretical loading distributions as calculated from reference 10 and from an unpublished extension of reference 10. Reference 10 is applicable to stations forward of the wing-root trailing edge, and the unpublished extension, to stations aft of the wing-root trailing edge. The theoretical curves, which are invariant with Mach number, are plotted with the data for Mach numbers of 0.90 and 1.05. The maximum values for the theoretical curves were higher than those for the flight data, and the shapes of the distributions were generally only approximated. Because it is assumed in the theory that the flow in each transverse plane perpendicular to the model center line is independent of the flow in adjacent planes, the slight forward spread of wing influence that occurred at subsonic speeds would, of course, not be predicted. For this reason, too, the aft movement with increasing Mach number of the minimum point in the vicinity of station 84 would not be predicted.

SUMMARY OF RESULTS

Free-fall tests have been made at small angles of attack and at Mach numbers from 0.85 to 1.06 of a wing-body configuration having a 45° swept wing on a fuselage of fineness ratio 12.4. The following significant results were obtained with regard to the distributions of loading over the model:

1. Through the test range of Mach numbers the fuselage in the vicinity of the wing carried a constant proportion of the total wing load amounting to 18 percent.

2. Predictions of the proportion of the load carried by the fuselage in the vicinity of the wing, based on subsonic and supersonic theories for a wing alone, agreed with experimental values within 12 percent for Mach numbers from 0.85 to 0.975 and at a Mach number of 1.05.

3. The portion of the fuselage forward of the wing carried a load additional to that carried by the fuselage in the vicinity of the wing amounting to about 12 percent of the total wing load.

4. The change in distribution of loading over the fuselage in the vicinity of the wing with increasing Mach number from 0.85 to 1.06 resulted in a 5-percent rearward movement of the wing aerodynamic center.

5. The distributions of loading over the fuselage in the vicinity of the wing were quite similar to the distributions measured in wind-tunnel tests of 45° swept wings having no camber and having ratios of wing chord to fuselage diameter different from that tested in flight.

Ames Aeronautical Laboratory
National Advisory Committee for Aeronautics
Moffett Field, Calif.

APPENDIX A

AIRSPEED CALIBRATION

The results of the calibration of the airspeed head shown in figure 4, as obtained by the radar method, are presented in figure 11 as a plot of $\Delta p/q_c$, against Mach number. The corrected Mach number variation with time as calculated using the curve of figure 11 is included in figure 5 for comparison with the recorded values.

Reference 11 presents the calibration of an identical airspeed head mounted in the same location on a similar body, but not having angle-of-attack and sideslip vanes. The calibration curve from reference 11 is reproduced in figure 11. It is apparent that there is a big difference in error which is attributable to the vanes. The differences in values of $\Delta p/q_c$, due to the vanes is shown in figure 12. Confirmation of the curve of figure 12 was obtained in flight tests conducted on an F-86A airplane in which the two airspeed heads, one with and the other without vanes, were mounted on booms extending 1-1/2-tip-chord lengths forward of each wing tip. The difference in recorded static pressure of the two heads, as determined from the F-86A tests, is plotted in figure 12 against airplane Mach number as determined from a calibrated airspeed installation. It should be noted that a direct comparison of the two curves of figure 12 is not strictly valid because the local Mach numbers at the airspeed heads on the F-86A were probably less than the airplane Mach numbers (reference 12). The corrections for these differences in Mach number are believed to be small enough so that the F-86A results can be interpreted as confirming the free-fall results at least up to a Mach number of about 1.01; the decrease in values for the free-fall-model tests at higher Mach numbers indicates the passage of the fuselage bow wave over the static orifices (reference 12).

REFERENCES

1. Delano, James B.: Pressure Distribution on the Fuselage of a Midwing Airplane Model at High Speeds. NACA TN 890, 1943.

2. Matthews, Clarence W.: Pressure Distributions Over a Wing-Fuselage Model at Mach Numbers of 0.4 to 0.99 and at 1.2. NACA RM L8H06, 1948.

3. Van Dyke, Milton D.: Aerodynamic Characteristics Including Scale Effect of Several Wings and Bodies Alone and in Combination at a Mach Number of 1.53. NACA RM A6K22, 1946.

4. Mayer, John P., and Gillis, Clarence L.: Division of Load Among the Wing, Fuselage, and Tail of Aircraft. NACA RM L51E14a, 1951.

5. Sutton, Fred B., and Martin, Andrew: Aerodynamic Characteristics Including Pressure Distributions of a Fuselage and Three Combinations of the Fuselage With Swept-Back Wings at High Subsonic Speeds. NACA RM A50J26a, 1951.

6. Loving, Donald L., and Estabrooks, Bruce B.: Transonic Wing Investigation in the Langley 8-Foot High-Speed Tunnel at High Subsonic Mach Numbers and at a Mach Number of 1.2. Analysis of Pressure Distribution of Wing-Fuselage Configuration Having a Wing of 45° Sweepback, Aspect Ratio 4, Taper Ratio 0.6, and NACA 65A006 Airfoil Section. NACA RM L51F07, 1951.

7. Zalovcik, John A.: A Radar Method of Calibrating Airspeed Installations on Airplanes in Maneuvers at High Altitudes and at Transonic and Supersonic Speeds. NACA TN 1979, 1949.

8. DeYoung, John, and Harper, Charles W.: Theoretical Symmetric Span Loading at Subsonic Speeds for Wings Having Arbitrary Plan Form. NACA Rep. 921, 1948. (Formerly issued as NACA TN's 1476, 1491, and 1772.)

9. Cohen, Doris: Theoretical Loading at Supersonic Speeds of Flat Swept-Back Wings with Interacting Trailing and Leading Edges. NACA TN 1991, 1949.

10. Spreiter, John R.; The Aerodynamic Forces on Slender Plane- and Cruciform-Wing and Body Combinations. NACA Rep. 962, 1950. (Formerly issued as NACA TN's 1662 and 1897.)

11. Selna, James: Preliminary Investigation of a Submerged Inlet and a Nose Inlet in the Transonic Flight Range With Free-Fall Models. NACA RM A51B14, 1951.

12. Thompson, Jim Rogers, Bray, Richard S., and Cooper, George E.: Flight Calibration of Four Airspeed Systems on a Swept-Wing Airplane at Mach Numbers Up to 1.04 by the NACA Radar-Phototheodolite Method. NACA RM A50H24, 1950.

TABLE I.- DIMENSIONS OF FREE-FALL MODEL

Gross weight, pounds	1316
Center of gravity	Station 100.5
Wing	
Area, square inches, S (including 315.4 sq in. projected through fuselage)	1291.7
Aspect ratio	6.0
Taper ratio	0.49
Sweepback, 1/4-chord line, degrees	45
Twist, washout at tip with respect to fuselage center line, streamwise, degrees	10
Incidence at center line, degrees	-0.17
Airfoil section, perpendicular to 1/4-chord line	NACA 64A810, a=0.8 (modified)
M.A.C., inches	15.19
Fuselage	
Ordinate at station x (x = 8.0 to x = 139.4), inches	$8.5\left[1-\left(\frac{x}{102}-1\right)^2\right]^{3/4}$
Fineness ratio	12.4

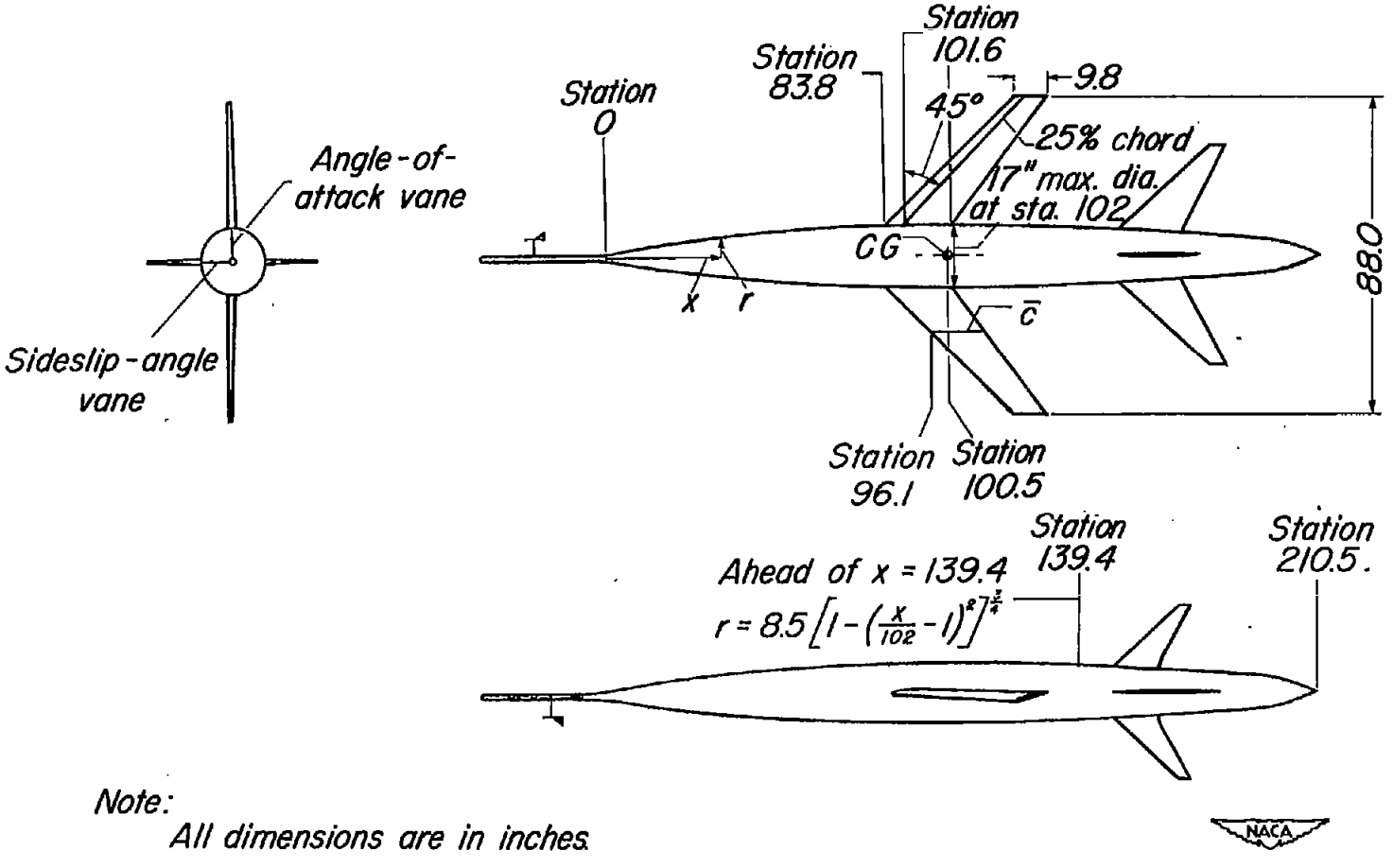

Note:
All dimensions are in inches

Figure 1. - Three-view drawing of free-fall model.

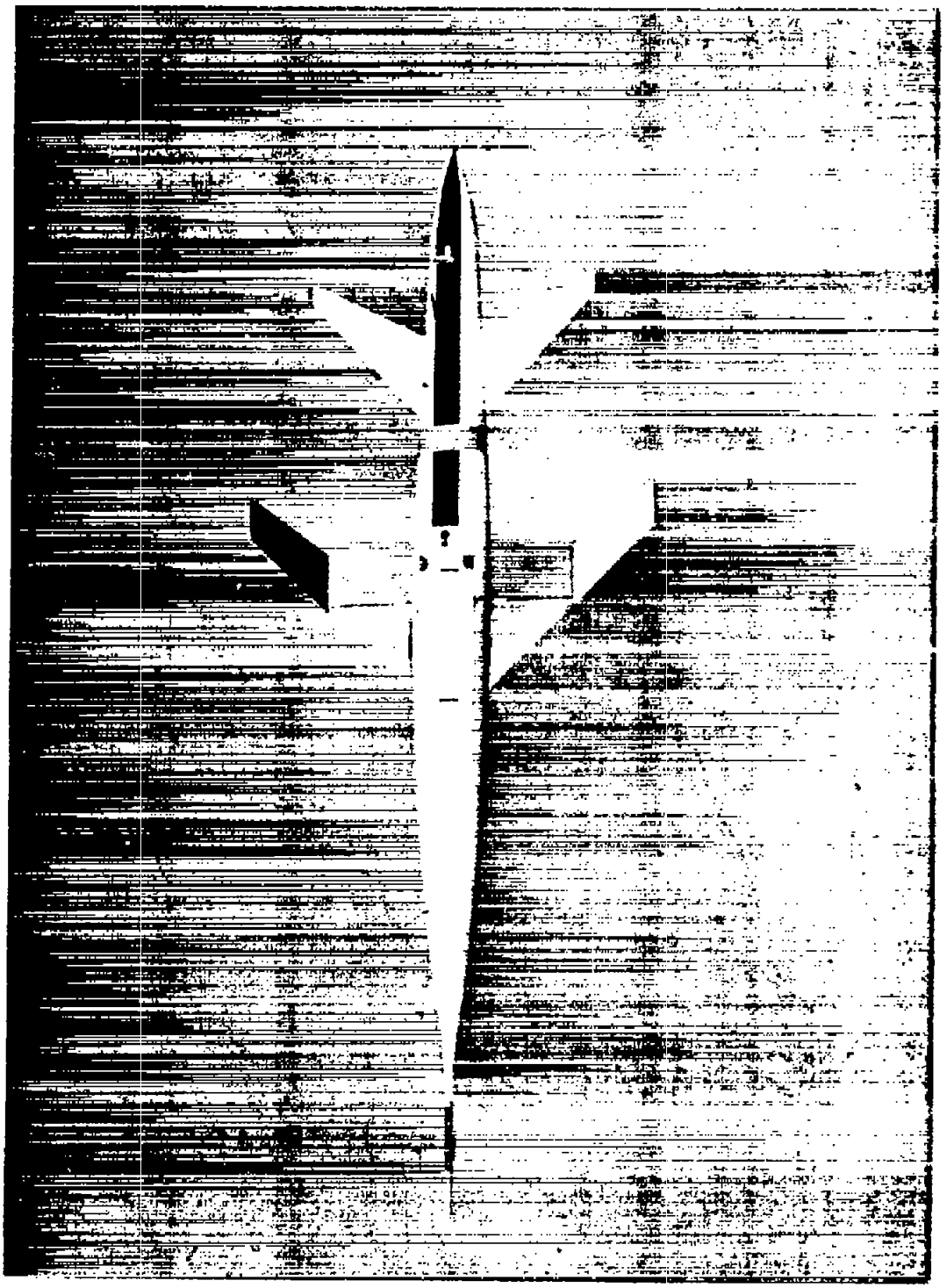

Figure 2.- Model in free fall immediately after release from carrier airplane.

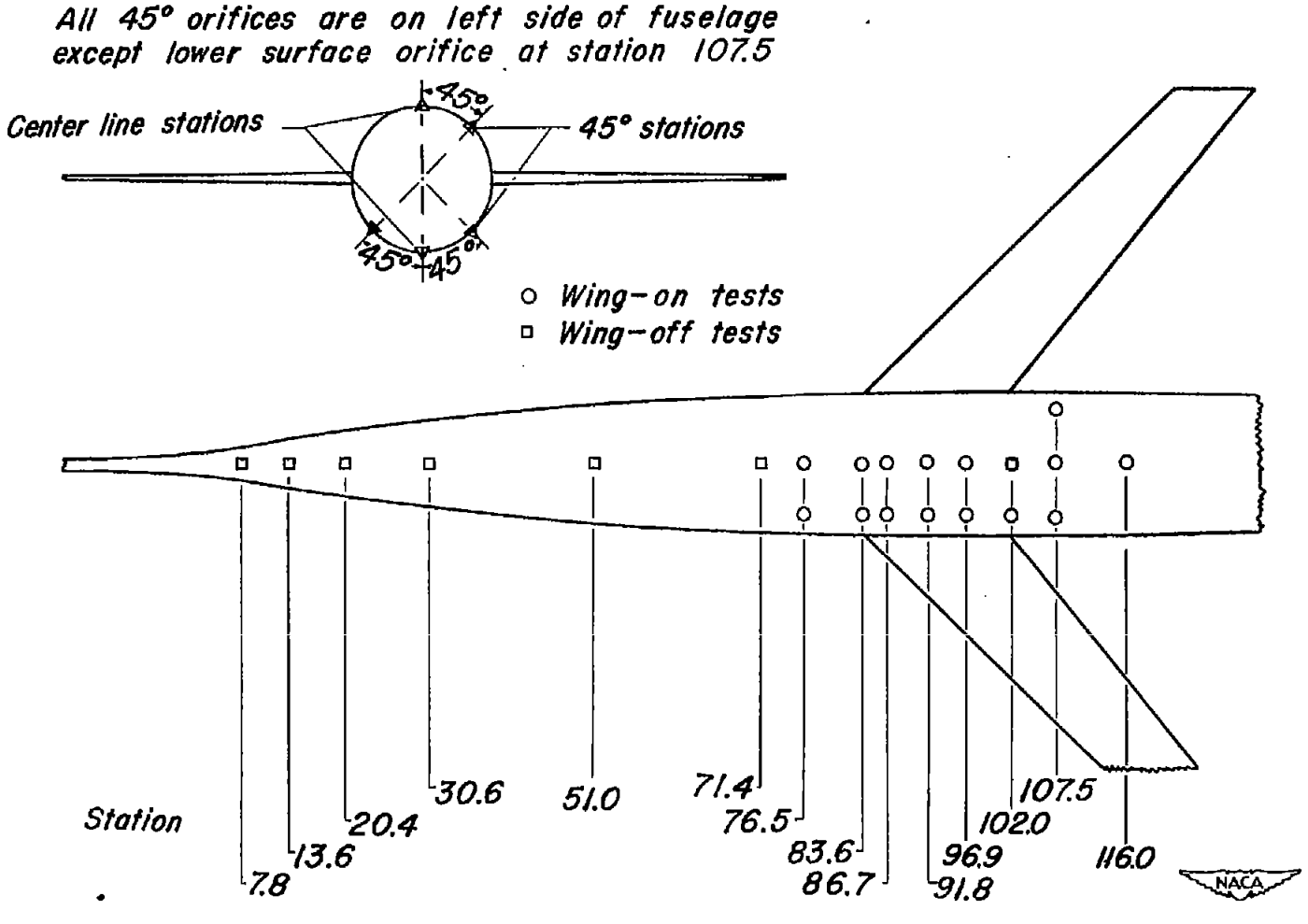

Figure 3. — Locations of pressure orifices on upper and lower surfaces of fuselage.

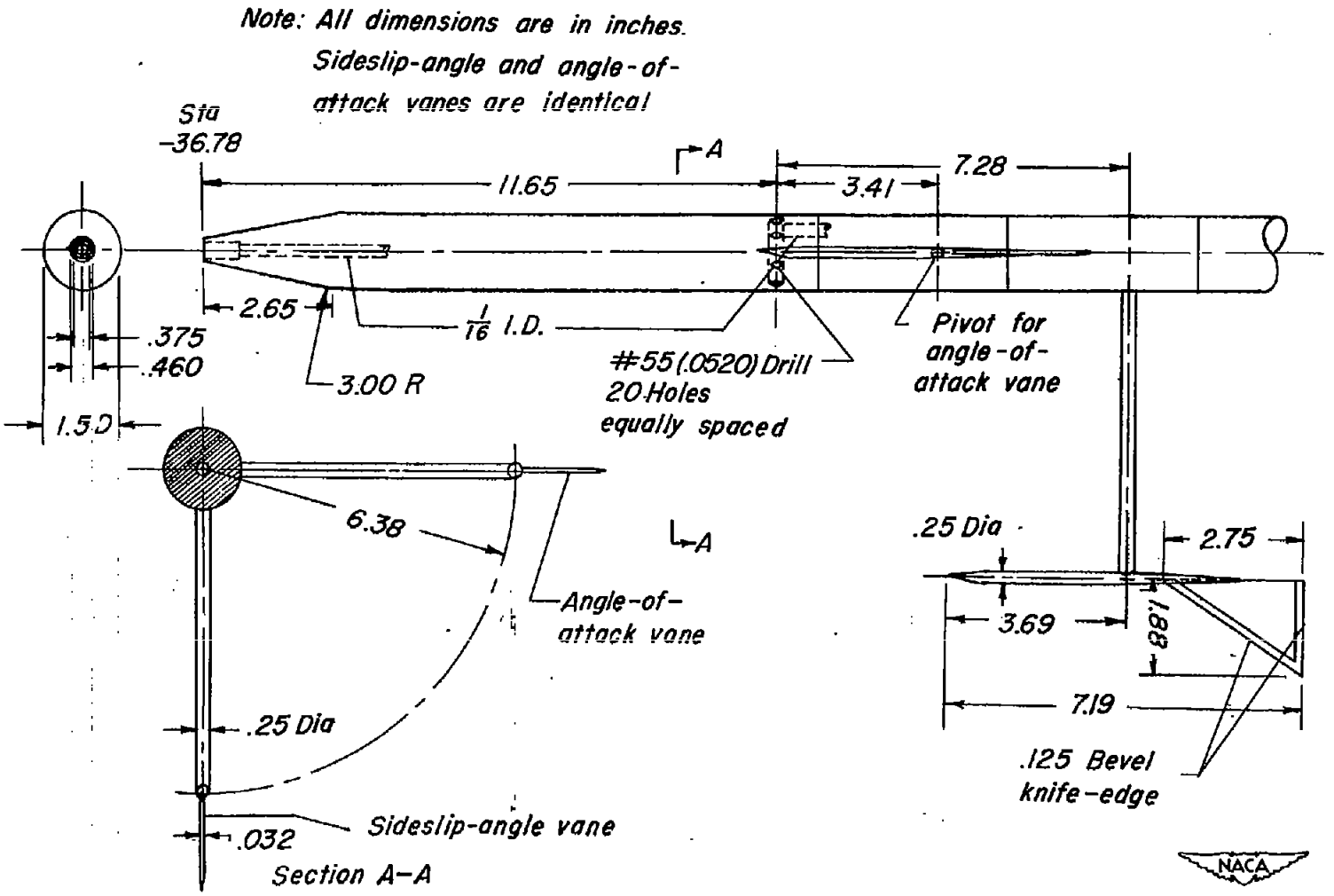

Figure 4.- Airspeed head, angle-of-attack vane, and sideslip-angle vane used on free-fall model.

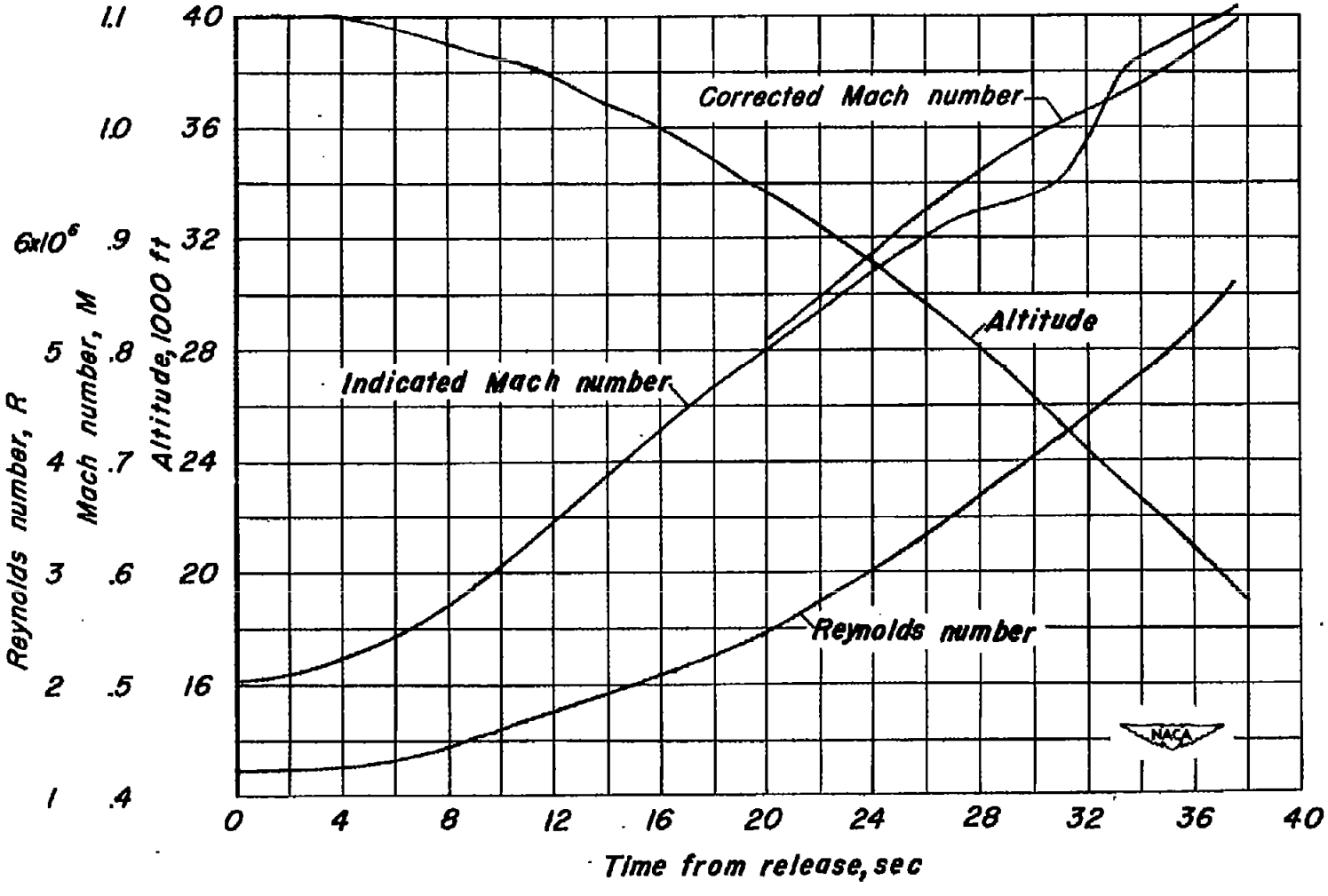

Figure 5.- Typical time history of altitude, Mach number, and Reynolds number during test period of drop.

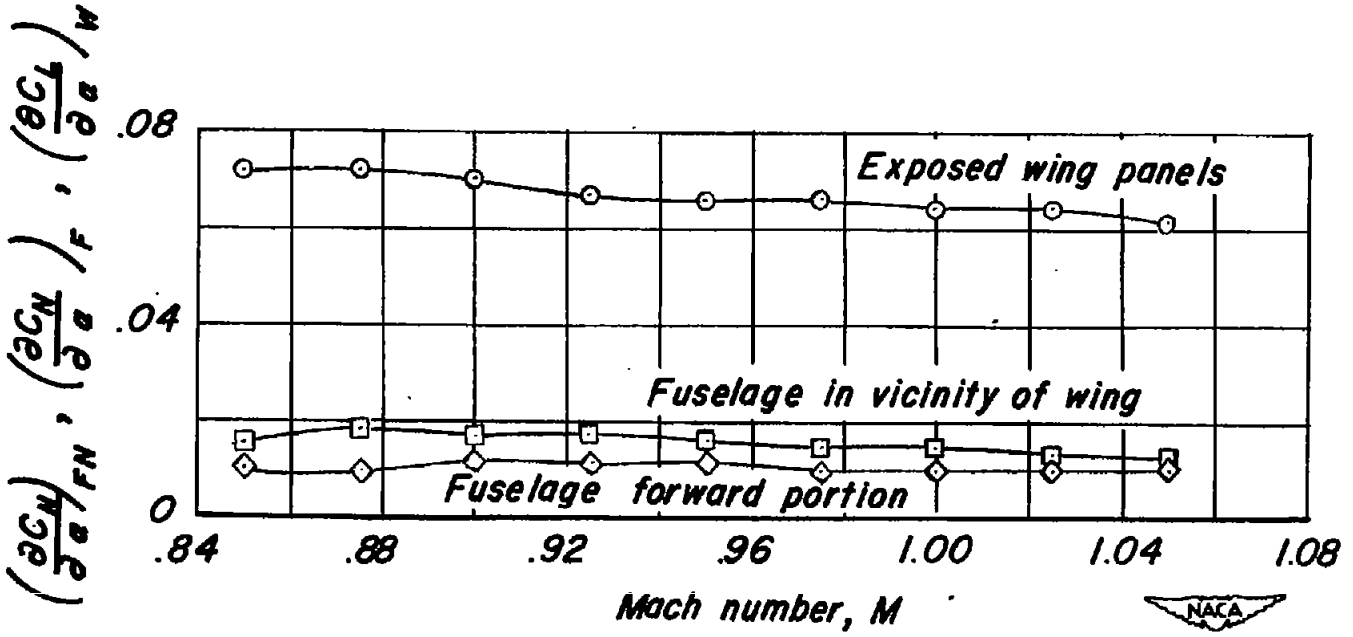

Figure 6.- Variation with Mach number of lift- and normal-force-curve slope for several portions of the free-fall model.

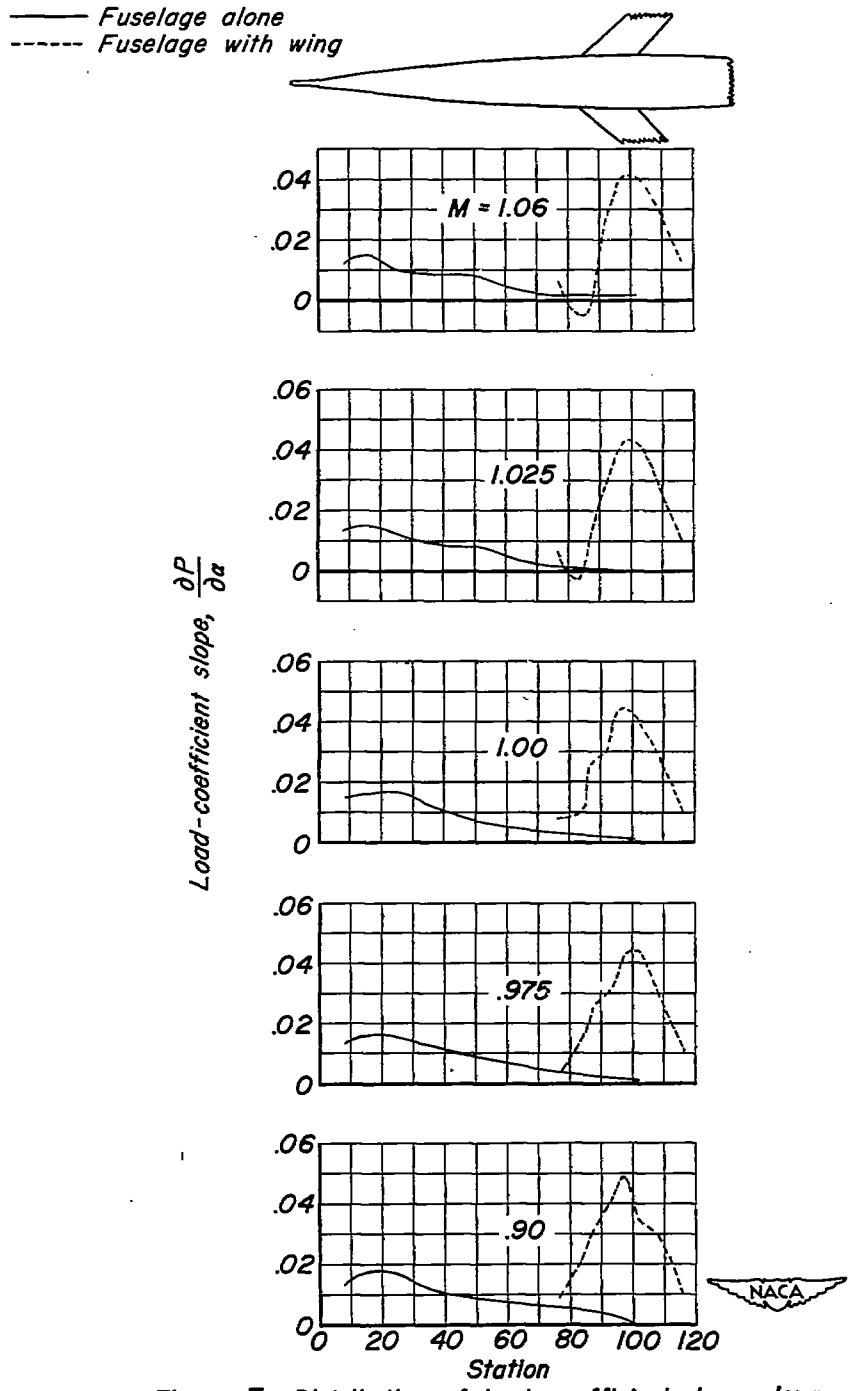

Figure 7.- Distribution of load-coefficient slope along center line of body, for fuselage alone and for fuselage in presence of wing.

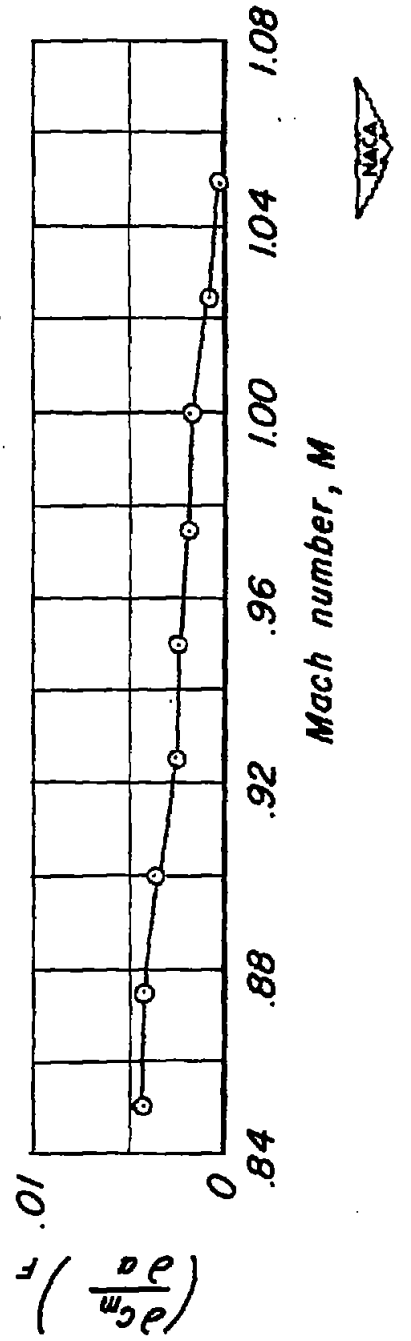

Figure 8.—Variation with Mach number of pitching-moment-coefficient slope due to loading over fuselage in vicinity of wing.

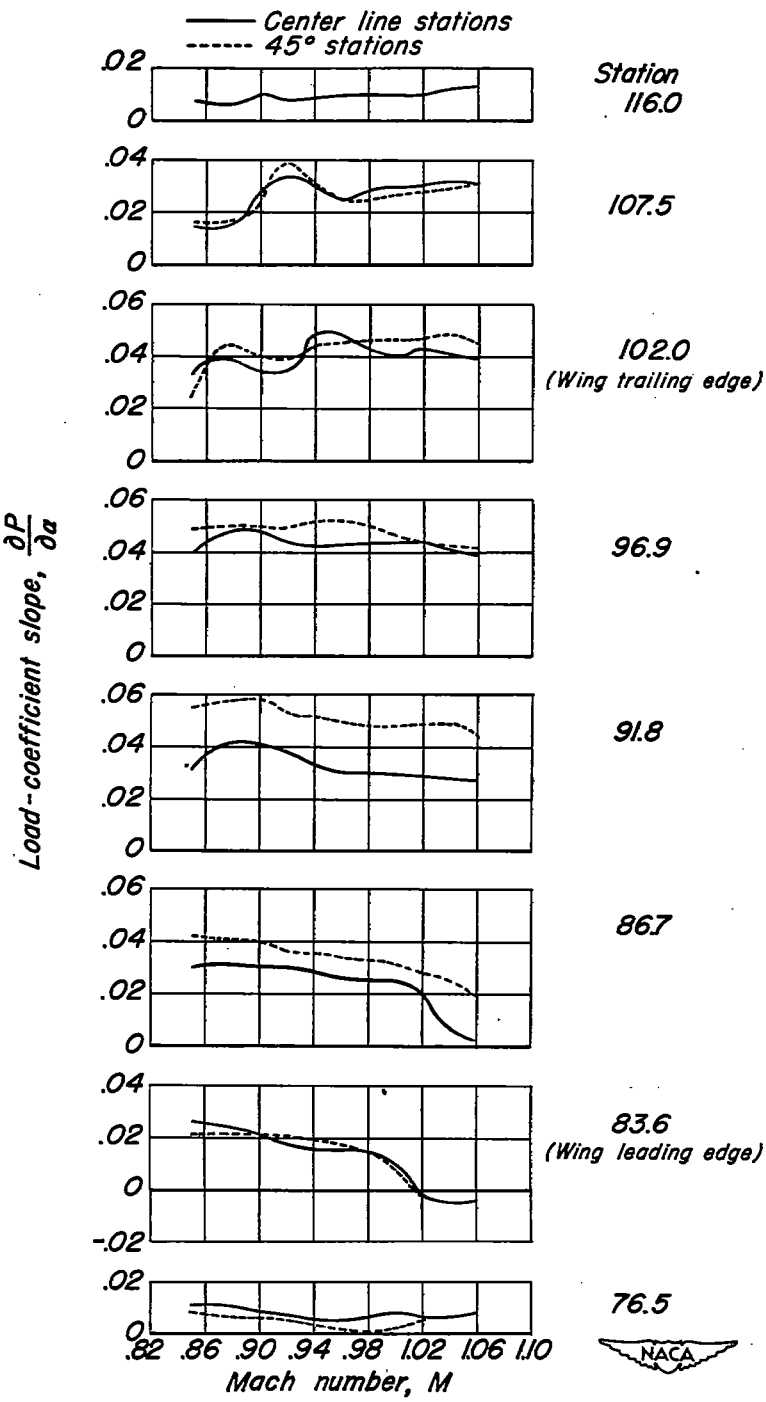

Figure 9.- Variation with Mach number of load-coefficient slope at measurement stations.

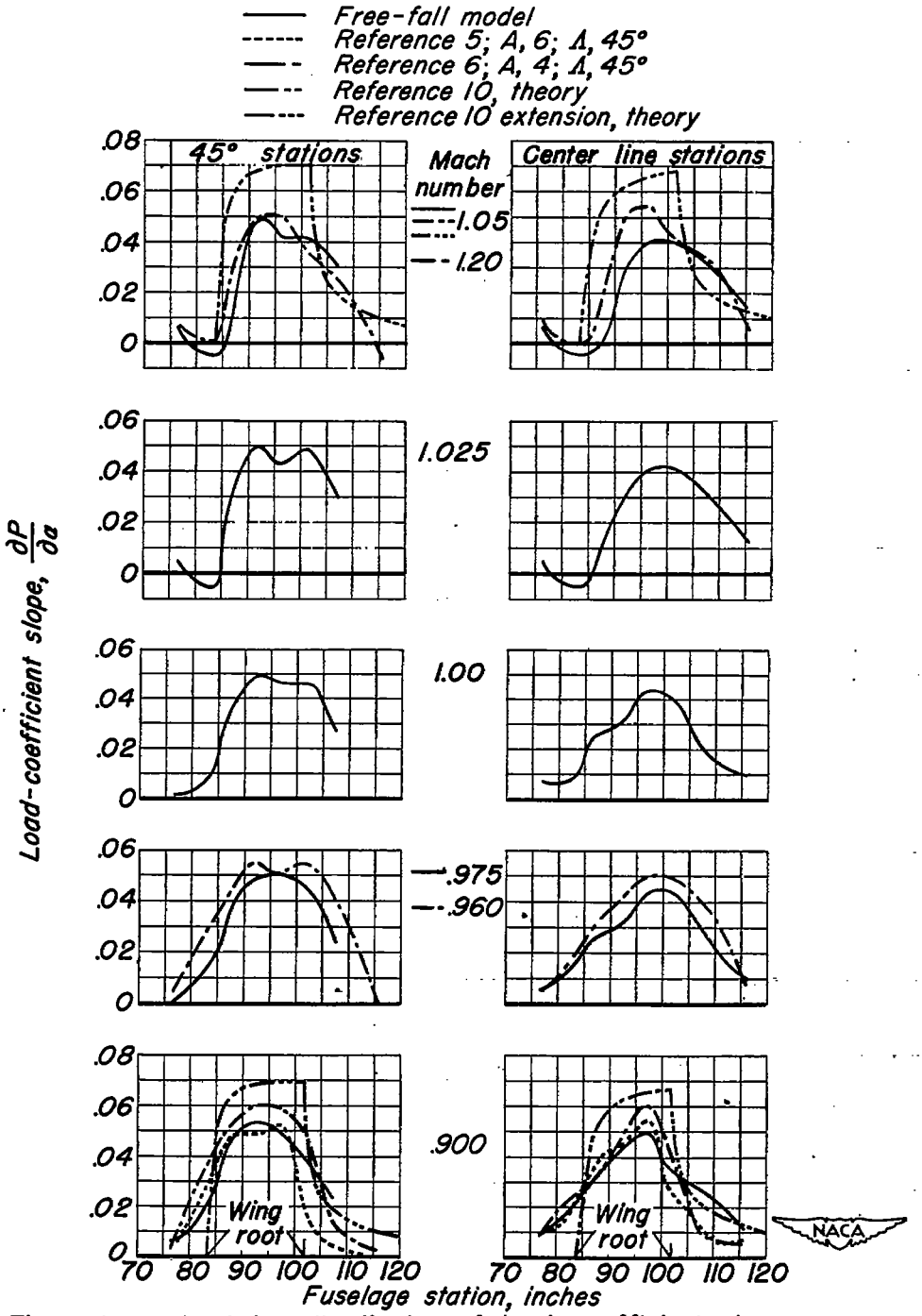

Figure 10. - Chordwise distribution of load-coefficient slope over fuselage in vicinity of wing at various transonic Mach numbers.

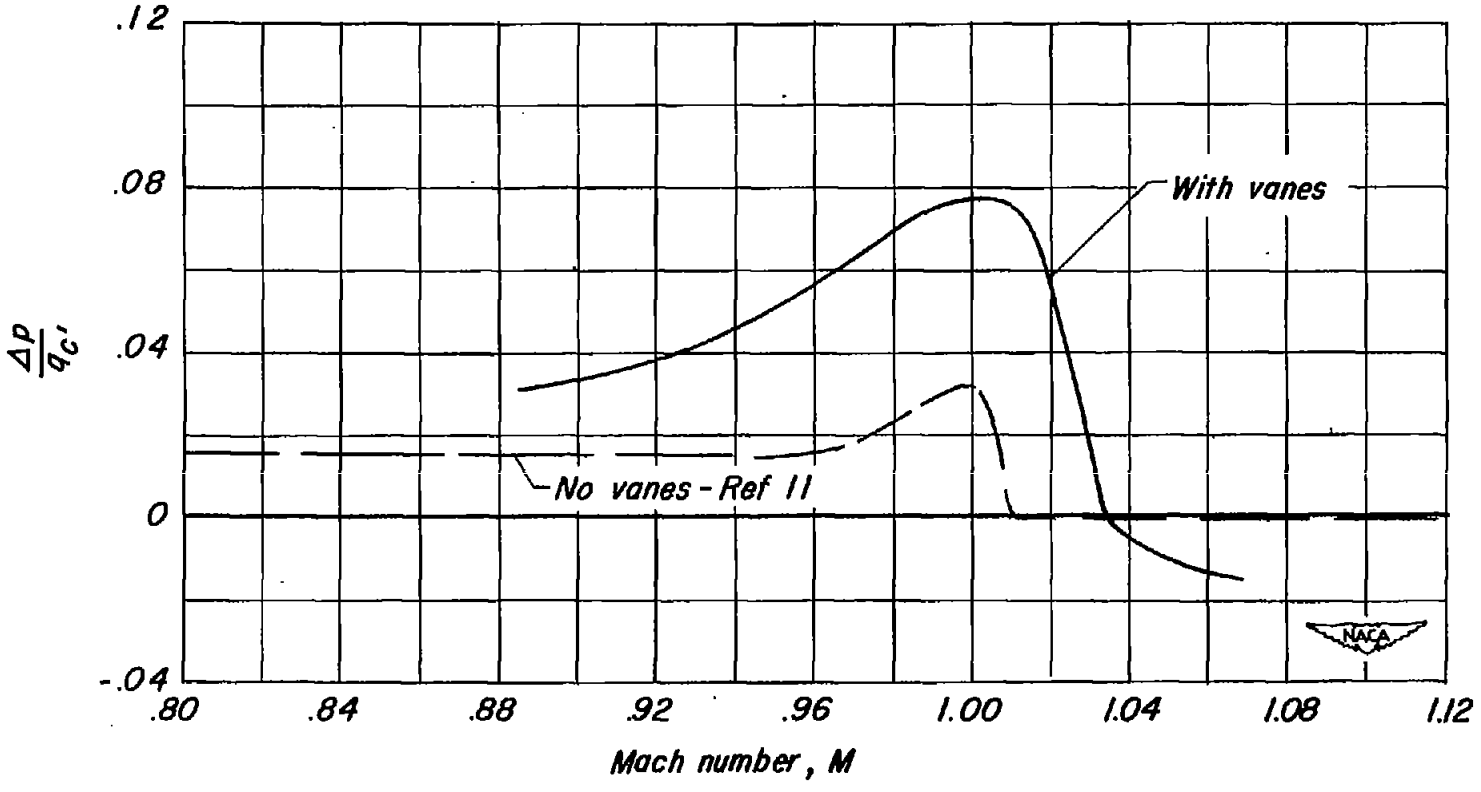

Figure 11.- Calibration of airspeed head mounted on nose of free-fall model.

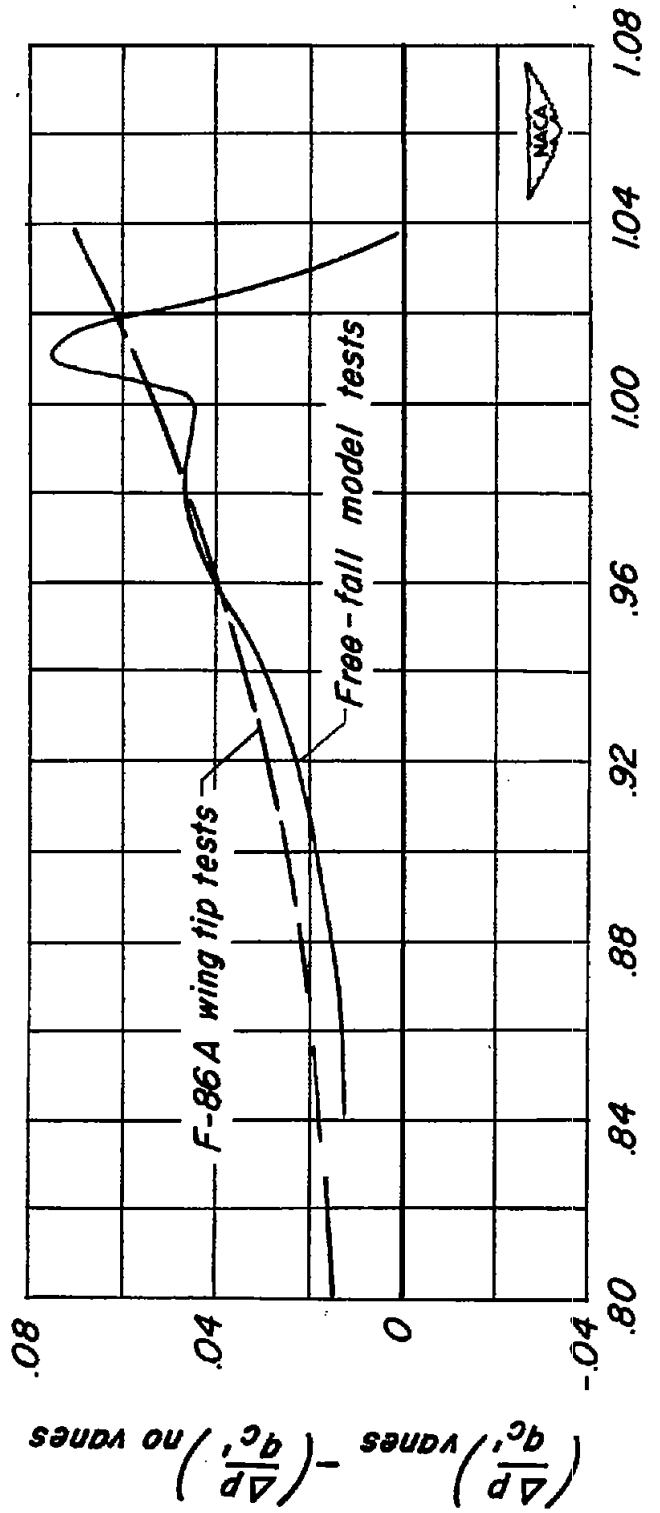

Figure 12.- Effect of vanes on calibration of airspeed heads used on free-fall models.

NACA-Langley - 11-27-51 - 400